Noname manuscript No.
(will be inserted by the editor)

Large oscillations of the trifilar pendulum: analytical and experimental study

G. Previati

Received: date / Accepted: date

Abstract The trifilar pendulum is one of the most widely used methods for the measurement of the moment of inertia of a body around a rotating axis. Despite its simplicity, this method allows very high accuracy.

In general, the motion of the pendulum is assumed to be small enough to be considered linear. However, some applications exist for which larger motions have to be employed. In these cases, the amplitude of the motion influences the period of oscillation of the pendulum and affects the moment of inertia measured value. To avoid such errors, the nonlinear motion of the pendulum in large oscillation conditions has to be considered. In this paper, the large motion of the pendulum is investigated analytically, numerically and experimentally. From these analyses, the situations where the nonlinearities of the motion of the pendulum have more influence on the accuracy are identified and described. The most important parameters influencing the period of oscillation are highlighted. The analyses show that by a proper and simple instrumentation of the pendulum, highly accurate results can be obtained also for large motion amplitudes. A calibration technique able to consider the most important nonlinearities in the motion of the pendulum is presented.

.

Keywords Moment of inertia measurement · Trifilar pendulum · Error analysis · Experimental calibration · Analytical study · Nonlinear motion

1 Introduction

The trifilar (or bifilar) pendulum technique is widely used in the measurement of the moment of inertia of rigid bodies around a rotation axis [16, 17, 19]. Although

G. Previati
Department of Mechanical Engineering, Politecnico di Milano
Tel.: +39-02-23998606
Fax: +39-02-23998263
E-mail: giorgio.previati@polimi.it
DOI: https://doi.org/10.1016/j.mechmachtheory.2020.104157

the method is very simple and non expensive hardware is involved, in the review presented in [19], the method has shown a high accuracy compared with other approaches with an uncertainty less than 1%.

The use of the trifilar pendulum is a well established practice and early papers dating back to the middle of the last century can be found [12]. In this paper, the trifilar pendulum is applied to military equipment. The paper presents the motion equation of the pendulum, derived for small amplitudes of oscillation. Also, an error analysis is presented where the error is computed by considering the sensitivity analysis of the linearized formula to each of its parameters. This approach for error estimation has been repeatedly applied to trifilar pendulums in several papers [20, 4, 3, 10, 8]. This kind of analysis has proved to be very useful to quantify the measurement error due to the principal parameters of the test rig, namely mass, cable lengths, distance between the cables and oscillation period. In [22], this analysis has been further developed to take into account the effects of the asymmetries in the construction of the pendulum.

The formula for the measurement of the moment of inertia is derived under the hypothesis of the centre of gravity of the system laying on the rotation axis of the pendulum. The error due to a misalignment of the centre of gravity has been also studied [3]. This error is mostly proportional to the square of the misalignment distance, and can be neglected in first order approximations of the error [3]. If the centre of gravity is purposely not aligned to the rotation axis, the pendulum can be used to measure the centre of gravity location [6]. The problem of avoiding lateral motions of the pendulum has also been investigated and centering devices to force pure rotational motions have been proposed [12, 18].

The motion of the trifilar pendulum evolves from a given initial displacement without further actuation. The damping of the motion is thus unavoidable. The damping problem has been considered since the most early papers [12]. In well-realized pendulums and in the absence of bodies with airfoil providing aerodynamic drag, the damping is usually small enough to consider negligible its effect on the oscillation period. In [11], the moments of inertia of an unmanned airplane are measured. In this case, the damping is not negligible and a nonlinear parameters identification procedure is employed to take its effects into account. Given the high damping of the airplane, large oscillation angles of the order of 25° have been imposed to the pendulum. A nonlinear motion equation has been considered to model the dependence of the oscillation period on damping and motion amplitude.

Referring to large oscillations of the pendulum, very few papers can be found in the literature discussing their effects. In [4], experimental tests are reported showing a non negligible influence of the oscillation amplitude on the measured period for amplitudes of the order of 5°. A quadratic interpolation is proposed to extrapolate the period for vanishing amplitudes. A rather complete analysis of the period dependency on the oscillation amplitude can be found in [6]. This paper shows that the sensitivity of the oscillation period on the amplitude strongly depends on the geometry of the pendulum and on the radius of gyration of the system. In particular, the period is more influenced by the oscillation amplitude if the distance between the cables is relatively large with respect to their length and if the radius of gyration of the system is small. In the paper, the nonlinear equations of motion of the pendulum are studied and a formula is proposed able to approximate the dependency of the period on the motion amplitude for most combinations of test rig geometry and radii of gyration. The formula gives a highly

non liner relationship between period and moment of inertia and seems not suitable for measurement purposes. In [7], also the effects of the centre of gravity offset are considered in non linear model. A study of the nonlinear motion of the pendulum is also proposed in [13] with the aim of reducing the measurement error below 1%. The proposed approach is, however, quite cumbersome and no significant improvement is found with respect to the standard linearized approach. In [14], a nonlinear approach is derived which has shown an accuracy of the order of 0.1% of the full scale of the employed test rig for non-small oscillation amplitudes, up to 45°. The approach is suitable for pendulums with long cables with respect to their distance or systems with a large radius of gyration.

Despite the few papers dealing with large oscillations, the possibility to perform measurements with arbitrary large amplitudes can be of relevant practical application. In fact, the measurement of the moment of inertia of compact bodies is prone to errors due to the period dependency on amplitude, even for small angles as shown in [4]. On the other hand, large bodies with airfoils are usually tested in large oscillations and in this case the length of the cables cannot be very large due to physical limitations. The present paper aims to study the large motion of the trifilar pendulum and derive a suitable procedure to its exploitation in actual measurements. The paper is structured as follows. Firstly, an analytical expression of the period as a function of the motion amplitude, pendulum geometry and inertia properties of the system is derived and numerically validated. Then, a measurement procedure for the moment of inertia based on this formula is shown and its effectiveness is proved by a numerical analysis. Finally, experimental tests are reported.

2 Oscillation period for large oscillations

The kinematics of the trifilar pendulum is depicted in Fig. 1. The carrying plate of the pendulum is depicted, for simplicity, as an equilateral triangle. The cables, of length L, are connected at the vertices of the triangle and are equidistant from the centre of the triangle, coincident with the centre of gravity of the system. The distance between the centre of gravity and the cable connection is R. In Fig. 1b, the rotation in the horizontal plane is shown. The pendulum rotates of an angle θ and the point A moves to the point A'. By simple trigonometric analysis, the distance $\overline{AA'}$ is $2R\sin\left(\frac{\theta}{2}\right)$.

Fig. 1b shows the motion of the pendulum in the vertical plane. Due to the rotation θ in the plane of the pendulum, the cables rotate of an angle α, while the plate moves upward of a quantity Δz. The displacement $\overline{AA'}$ is equal to $L\sin\alpha$. By equating the distance $\overline{AA'}$ computed in the horizontal and in the vertical plane, the relationship between θ and α reads

$$L\sin\alpha = 2R\sin\left(\frac{\theta}{2}\right) \tag{1}$$

The displacement Δz can be computed as function of α as

$$\Delta z = L\left(1-\cos\alpha\right) \tag{2}$$

and by remembering eq. 1, as function of θ as

$$\Delta z = L - \sqrt{L^2 - 4R^2 \sin^2\left(\frac{\theta}{2}\right)} = L - \sqrt{L^2 - 2R^2 + 2R^2\cos\theta} \tag{3}$$

The potential energy of the system is given by two contributions, the potential energy of the mass m of the system moving in the vertical direction and the elastic energy of the structural torsional system of the pendulum. The torsional stiffness can be present if the cables are clamped to the plate and no spherical joint is present. In most systems, a spherical joint is applied in order to avoid this torsional system. However, such spherical joints complicate the hardware of the system and have a (small) friction. If the torsional stiffness is considered, a simpler hardware can be realized and the friction is avoided. Taking into account these two contributions, the potential energy reads

$$U = mg\Delta z + \frac{1}{2}k\theta^2 = mg\left(L - \sqrt{L^2 - 2R^2 + 2R^2\cos\theta}\right) + \frac{1}{2}k\theta^2 \tag{4}$$

where g is the acceleration of gravity and k the torsional stiffness. m is the mass of the system, given by the sum of the mass of the carrying plate (m_0) and of the mass of the body under investigation (m_1), i.e. $m = m_0 + m_1$.

The kinetic energy of the system is given by the vertical motion of the mass of the system and by the rotational motion of the inertia J of the system and reads

$$E = \frac{1}{2}m\Delta\dot{z}^2 + \frac{1}{2}J\dot{\theta}^2 = \frac{1}{2}m\left(\frac{d\left(\Delta z\right)}{d\theta}\dot{\theta}\right)^2 + \frac{1}{2}J\dot{\theta}^2 \tag{5}$$

with

$$\frac{d\left(\Delta z\right)}{d\theta} = \frac{R^2\sin\theta}{\sqrt{L^2 - 2R^2 + 2R^2\cos\theta}} \tag{6}$$

J is the inertia of the system, given by the sum of the inertia of the carrying plate (J_0) and of the inertia of the body under investigation (J_1), i.e. $J = J_0 + J_1$. It has to be observed, that this relationships implies that the carrying plate and the body under investigation have their centre of gravity lying on the vertical axis passing through the centre of the plate. This simplification does not reduce the generality of the following analysis as it is always possible to add balancing masses in order to achieve such distribution. Moreover, in general, the carrying plate is designed to have its centre of gravity in this position and absolute care is given in mounting the body under investigation with the same requirement, in case adding balancing masses.

The equation of motion can be obtained by differentiating the potential and kinetic energy of the system as

$$\begin{aligned} &\left(J + \frac{mR^4\sin^2\theta}{L^2 - 2R^2 + 2R^2\cos\theta}\right)\ddot{\theta} + \\ &+\frac{mR^2\sin\theta\left(R^2 + R^2\cos^2\theta + L^2\cos\theta - 2R^2\cos\theta\right)}{\left(L^2 - 2R^2 + 2R^2\cos\theta\right)^2}\dot{\theta}^2 + \\ &+\frac{mgR^2\sin\theta}{\sqrt{L^2 - 2R^2 + 2R^2\cos\theta}} + k\theta = 0 \end{aligned} \tag{7}$$

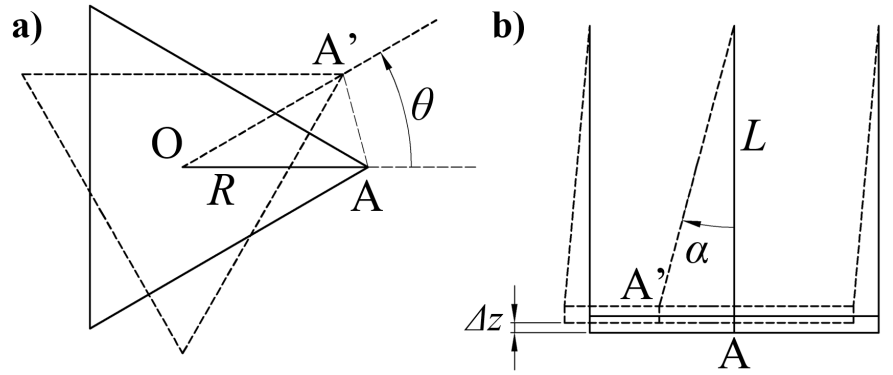

Fig. 1: Trifilar pendulum kinematic. O is the geometrical centre of the pendulum, R is the distance between the centre and each cable. a) Top view. b) Lateral view.

In eq. 7 the dissipation terms have not been considered. In fact, if no aerodynamic effect is present to damp the system, the pendulum is realized in order to minimize friction and other sources of damping. Thus, for usual applications, damping is negligible.

The obtained equation of motion (eq. 7) is a non linear function of the sole coordinate θ describing the rotation of the pendulum. For θ small, Eq. 7 can be linearized as

$$J\ddot{\theta} + \left(\frac{mgR^2}{L} + k\right)\theta = 0 \tag{8}$$

with oscillation period

$$T = 2\pi\sqrt{\frac{J}{\frac{mgR^2}{L} + k}}, \tag{9}$$

which for $k = 0$ leads to the well known formula for the period of the trifilar pendulum

$$T = 2\pi\sqrt{\frac{JL}{mgR^2}} \tag{10}$$

For non small oscillations, eq. 7 can be approximated with its Taylor series up to the fourth order as

$$\begin{aligned}\left(J + \frac{mR^4\theta^2}{L^2}\right)\ddot{\theta} + \frac{Rm^4}{L^2}\theta\dot{\theta}^2 + \\ + \left(\frac{mgR^2}{L} + k\right)\theta - \frac{mgR^2}{L}\left(\frac{1}{6} - \frac{R^2}{2L^2}\right)\theta^3 = 0\end{aligned} \tag{11}$$

Calling

$$A = \frac{mR^4}{L^2} \tag{12}$$

$$B = \frac{mgR^2}{L} \tag{13}$$

$$C = \frac{1}{6} - \frac{R^2}{2L^2} \tag{14}$$

eq. 11 can be rewritten as

$$\left(J + A\theta^2\right)\ddot{\theta} + A\theta\dot{\theta}^2 + (B + k)\,\theta - BC\theta^3 = 0 \tag{15}$$

The oscillation period can be derived by following the procedure presented in [1]. Knowing that the physical solution of the system is an oscillation, a test function of the kind $\theta_0 \cos(\omega t)$ can be employed. θ_0 represents the motion amplitude, ω the angular frequency and t is the time. By substituting the test function in eq. 15 the following relationship is obtained

$$\begin{aligned}\left(J + A\theta_0^2 \cos^2(\omega t)\right)\left(-\theta_0\omega^2 \cos(\omega t)\right) + \\ + A\omega^2\theta_0^3 \cos(\omega t)\left(-\sin(\omega t)\right)^2 + \\ + (B + k)\,\theta_0 \cos(\omega t) - BC\theta_0^3 \cos^3(\omega t) = 0\end{aligned} \tag{16}$$

$\cos^3(\omega t)$ and $\cos(\omega t)\sin^2(\omega t)$ ca be approximated as

$$\cos^3(\omega t) = \frac{3}{4}\cos(\omega t) + \frac{1}{4}\cos(3\omega t) \approx \frac{3}{4}\cos(\omega t) \tag{17}$$

$$\cos(\omega t)\sin^2(\omega t) = \frac{1}{4}\cos(\omega t) - \frac{1}{4}\cos(3\omega t) \approx \frac{1}{4}\cos(\omega t) \tag{18}$$

where the terms referring to higher frequencies have been neglected. By substituting eq. 17 and eq. 18 in eq. 16 and rearranging, eq. 16 can be rewritten as

$$-\theta_0\omega^2 \cos(\omega t)\left(J + \frac{1}{2}A\theta_0^2\right) + \theta_0 \cos(\omega t)\left(k + B\left(1 + \frac{3}{4}C\theta_0^2\right)\right) = 0 \tag{19}$$

An by simplifying $\theta_0 \cos(\omega t)$

$$\omega^2\left(J + \frac{1}{2}A\theta_0^2\right) - \left(k + B\left(1 + \frac{3}{4}C\theta_0^2\right)\right) = 0 \tag{20}$$

From eq. 20, the oscillation period for large oscillations results

$$T = 2\pi\sqrt{\frac{J + \frac{1}{2}A\theta_0^2}{k + B\left(1 + \frac{3}{4}C\theta_0^2\right)}} \tag{21}$$

that for θ_0 small reduces to eq. 9.

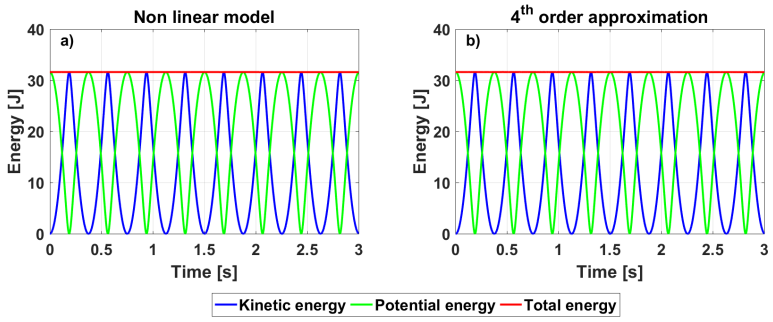

Fig. 2: Energy balance during the simulation of the motion of the pendulum. Initial oscillation angle 45^o, $R/L = 0.5$, data in Table 1. a) Non linear model of eq. 7. b) Fourth order approximation of eq. 11.

2.1 Numerical validation

In this section a multibody model of the trifilar pendulum is used for the validation of the formula of eq. 21 for the computation of the pendulum period. The considered multibody model is realized by Matlab Simmechanics™and comprises a plate, the body under investigation, three massless rigid cables and a torsional stiffness representing the clamping of the cables. The multibody model is simple and reproduces the system of Fig. 1 in order to evaluate eq. 21 under the same modelling hypotheses. Table 1 reports the parameters used for the simulations. The torsional stiffness of the cables in the table has been estimated by considering length, section and fill factor of the cables.

Usual trifilar pendulum applications, have a small ration R/L in order to keep the motion as close to a linear situation as possible. In this analysis, to test the ability of eq. 21 to catch the nonlinear behavior of the system, the ratio R/L is varied from a small value of 0.1 to a very large value of 1.

A preliminary numerical validation is also reported in Fig. 2. The figure shows the energy balance during a simulation with an initial rotation angle of 45^o and $R/L = 0.5$. Both the complete non linear model of eq. 7 and the approximated fourth order model of eq. 11 show a constant value of the total energy.

Fig. 3 shows the comparison between the period of oscillation computed by the multibody model and the approximated formula of eq. 21. In Fig. 3a, the simulations have been performed with the data in Table 1 for motion amplitudes from 1^o to 45^o. In Fig. 3b and 3c, the same simulations have been performed with the mass increased four times (i.e. half of the radius of gyration) and decreased four times (i.e. double of the radius of gyration) respectively. The pictures show that eq. 21 is able to approximate the oscillation period in all the considered condition, even when the nonlinear effects change the period value of about 12 times. The difference between the period computed by the multibody model and eq. 21 is always below the 10% of the computed period as shown in Fig. 4, with much smaller errors when R/L is small or as the radius of gyration grows.

While Fig. 3 shows that eq. 21 is able to approximate the period, it also shows that the error in the prediction of the period is not acceptable for a direct uti-

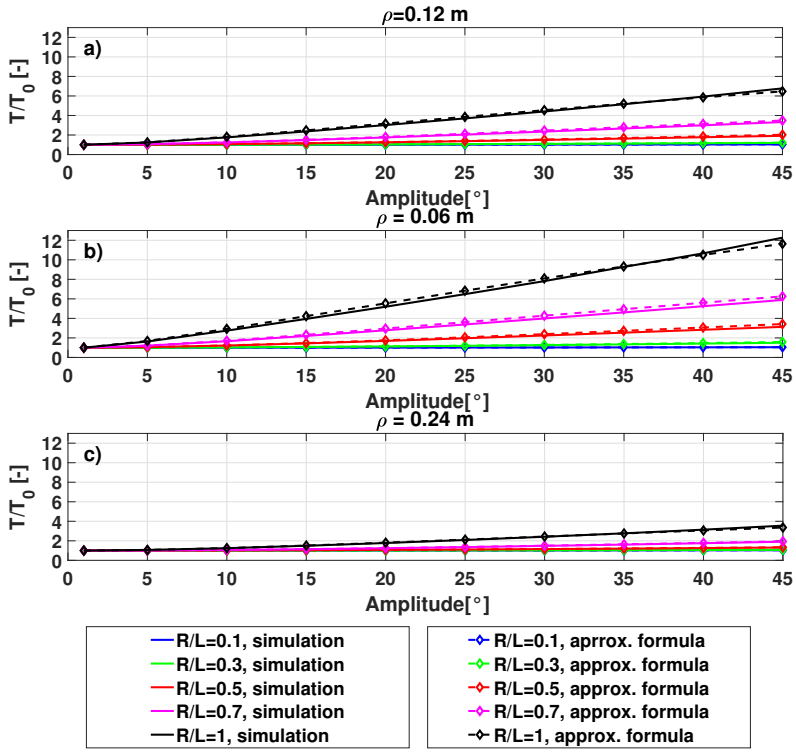

Fig. 3: Oscillation periods of the trifilar pendulum for different motion amplitudes computed by the multibody model and by the approximated formula of eq. 21. a) Simulations with data of Table 1. b) Mass increased four times. c) Mass decreased four times.

Table 1: Simulation data

Parameter	Value
Mass of the carrying plate (m_0)	5 kg
Mass of the body under investigation (m_1)	23.203 kg
Moment of inertia of the carrying plate (J_0)	0.1 kgm^2
Moment of inertia of the body under investigation (J_1)	0.3035 kgm^2
Radius of gyration of the system (ρ)	0.12 m
Length of the cables (L)	1.5 m
Diameter of the cables	1.5 mm
Fill factor of the cables	0.6
Torsional stiffness of the cables (k)	0.05 Nm

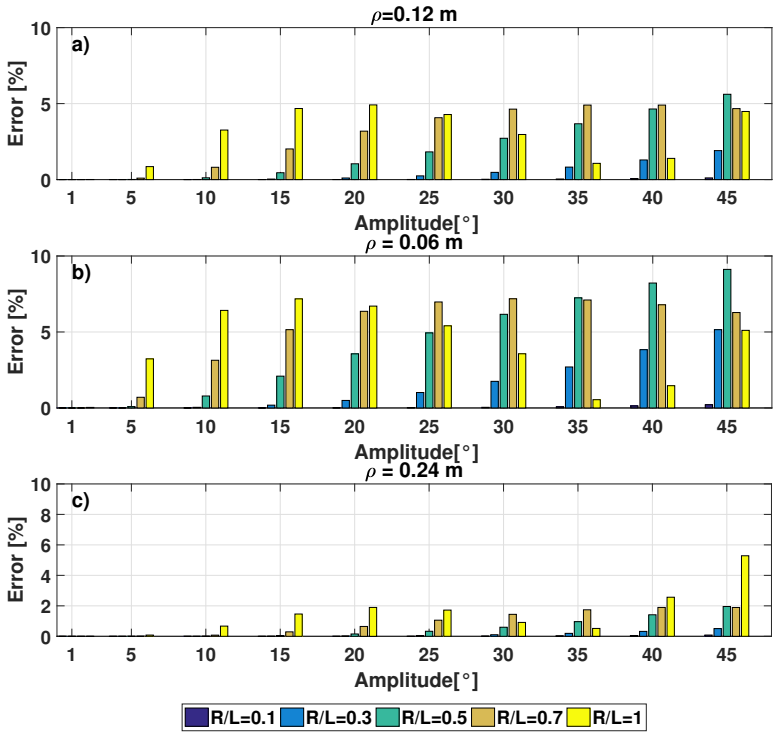

Fig. 4: Oscillation period errors of the approximated formula of eq. 21. a) Simulations with data of Table 1. b) Mass increased four times. c) Mass decreased four times.

lization of eq. 21 for the measurement of the moment of inertia. In fact, for some combination of the parameters, given approximation error in the period, a direct inversion of eq. 21 will lead to large errors in the measurement of the moment of inertia. A calibration procedure is thus necessary.

3 Calibration procedure

This section aims to the definition of a calibration procedure, based on eq. 21, for the measurement of the moment of inertia of a rigid body by the trifilar pendulum in large oscillations. The proposed procedure is based on the one presented in [18], but with significant differences due to the large oscillations here considered.

By algebraic manipulation of eq. 21, the following expression of the moment of inertia can be derived

$$J = -\frac{1}{2}A\theta_0^2 + \frac{BT^2}{4\pi^2}\left(1 + \frac{3}{4}C\theta_0^2\right) + \frac{kT^2}{4\pi^2} \tag{22}$$

By remembering $m = m_0 + m_1$, $J = J_0 + J_1$ and the expressions of A and B (eq. 12 and eq. 13), from eq. 22 the moment of inertia J_1 of the body under investigation can be computed as

$$\begin{aligned} J_1 = -J_0 - \frac{m_0 R^4 \theta_0^2}{L^2} - \frac{R^4\theta_0^2}{L^2}m_1 + \\ + \left(\frac{m_0 g R^2}{4\pi^2}\left(1 + \frac{3}{4}C\theta_0^2\right) + \frac{k}{4\pi^2}\right)T^2 + \frac{gR^2}{4\pi^2}\left(1 + \frac{3}{4}C\theta_0^2\right)m_1 T^2 \end{aligned} \tag{23}$$

By defining

$$P_1(\theta_0) = -J_0 - \frac{m_0 R^4 \theta_0^2}{L^2} \tag{24}$$

$$P_2(\theta_0) = -\frac{R^4\theta_0^2}{L^2} \tag{25}$$

$$P_3(\theta_0) = \frac{m_0 g R^2}{4\pi^2}\left(1 + \frac{3}{4}C\theta_0^2\right) + \frac{k}{4\pi^2} \tag{26}$$

$$P_4(\theta_0) = \frac{gR^2}{4\pi^2}\left(1 + \frac{3}{4}C\theta_0^2\right) \tag{27}$$

eq. 23 can be rewritten as

$$J_1 = P_1(\theta_0) + P_2(\theta_0)\, m_1 + P_3(\theta_0)\, T^2 + P_4(\theta_0)\, m_1 T^2 \tag{28}$$

Eq. 28 is a key achievement of the paper. This equation shows that the moment of inertia is a linear function of the quantities m_1, T^2 and m_1T^2. With respect to the similar expression found in [18], the additional quantity m_1 has been identified. Also, the four coefficients of eq. 28 are not constant but depend on the oscillation amplitude θ_0. From a calibration point of view, this means that the calibration tests and the actual measurements have all to be performed for the same motion amplitude.

For small angles, eq. 28 reduces to

$$J_1 = -J_0 + \left(\frac{(m_0 + m_1)gR^2}{4\pi^2} + \frac{k}{4\pi^2}\right)T^2 \tag{29}$$

Eq. 29 is composed by the well known formula for the computation of the moment of inertia from the measurement of the period for small oscillations plus the contribution of the torsional stiffness of the cables (if to be considered).

From eq: 28 and by supposing to measure n bodies ($n \geq 4$) with known mass m_i, $i = 1...n$, and inertia J_i, $i = 1...n$, the following linear system can be written

$$\begin{aligned} J_1 &= P_1\left(\overline{\theta_0}\right) + P_2\left(\overline{\theta_0}\right) m_1 + P_3\left(\overline{\theta_0}\right) T_1^2 + P_4\left(\overline{\theta_0}\right) m_1 T_1^2 \\ J_2 &= P_1\left(\overline{\theta_0}\right) + P_2\left(\overline{\theta_0}\right) m_2 + P_3\left(\overline{\theta_0}\right) T_2^2 + P_4\left(\overline{\theta_0}\right) m_2 T_2^2 \\ &\vdots \\ J_n &= P_1\left(\overline{\theta_0}\right) + P_2\left(\overline{\theta_0}\right) m_n + P_3\left(\overline{\theta_0}\right) T_n^2 + P_4\left(\overline{\theta_0}\right) m_n T_n^2 \end{aligned} \tag{30}$$

where $\overline{\theta_0}$ is the motion amplitude equal for all tests. Eq. 30 can be rewritten in matrix form as

$$\mathbf{b} = \mathbf{K}\mathbf{a} \tag{31}$$

being

$$\mathbf{b} = \begin{bmatrix} J_1 \\ J_2 \\ \vdots \\ J_n \end{bmatrix}, \quad \mathbf{K} = \begin{bmatrix} 1 & m_1 & T_1^2 & m_1 T_1^2 \\ 1 & m_2 & T_2^2 & m_2 T_2^2 \\ \vdots & \vdots & \vdots & \vdots \\ 1 & m_n & T_n^2 & m_n T_n^2 \end{bmatrix}, \quad \mathbf{a} = \begin{bmatrix} P_1\left(\overline{\theta_0}\right) \\ P_2\left(\overline{\theta_0}\right) \\ P_3\left(\overline{\theta_0}\right) \\ P_4\left(\overline{\theta_0}\right) \end{bmatrix} \tag{32}$$

The vector of the estimated parameters $\widehat{\mathbf{a}} = \left[\widehat{P_1}\left(\overline{\theta_0}\right)\ \widehat{P_2}\left(\overline{\theta_0}\right)\ \widehat{P_3}\left(\overline{\theta_0}\right)\ \widehat{P_4}\left(\overline{\theta_0}\right)\right]^T$ can be obtained from the solution of the system of eq. 31 as [2]

$$\widehat{\mathbf{a}} = \left(\mathbf{K}^T\mathbf{K}\right)^{-1}\mathbf{K}^T\mathbf{b} \tag{33}$$

and the measured moment of inertia J_b of the body under investigation of mass m_b is given by

$$J_b = \widehat{P_1}\left(\overline{\theta_0}\right) + \widehat{P_2}\left(\overline{\theta_0}\right) m_b + \widehat{P_3}\left(\overline{\theta_0}\right) T_b^2 + \widehat{P_4}\left(\overline{\theta_0}\right) m_b T_b^2 \tag{34}$$

where T_b is the measured period of oscillation for the body at the oscillation amplitude $\overline{\theta_0}$

3.1 Coefficients sensitivity analysis

In Fig. 5, the percentage difference in the moments of inertia if computed by eq. 29 (expression of the moment of inertia for small oscillation angles) or by eq. 28 (expression of the moment of inertia for large oscillation angles) is depicted as function of motion amplitude. The graphs have been derived for four combination of the radius of gyration (ρ) and of the ration R/L. In each graph, the contribution of each term of eq. 28 is indicated in a different color (expressions of the coefficients in eq.s 24-27).

The figure shows that the percentage difference in the computation of the moment of inertia by the two formulae increases as the radius of gyration decreases and the ration R/L increases, i.e the difference increases as the dependence of the period on the motion amplitude is more relevant (see also Fig. 3). When a large radius of gyration or a small ratio R/L is considered, most of the difference is due to the terms $P_3(\theta_0)$ and $P_4(\theta_0)$ (Fig. 5a, 5c and 5d). These two terms are

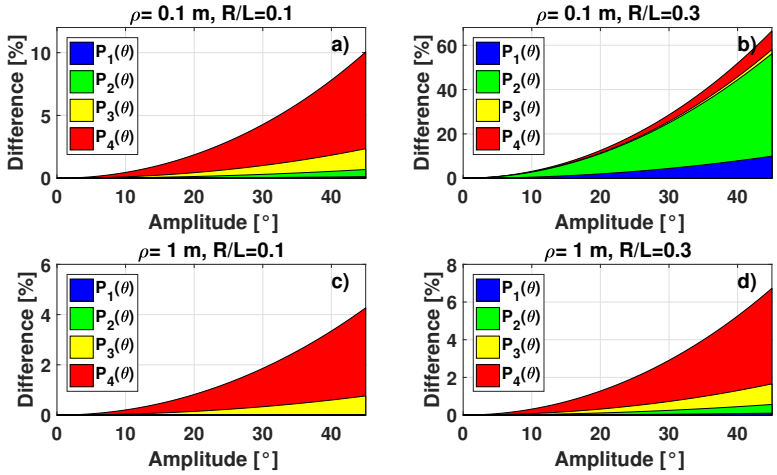

Fig. 5: Percentage difference in the moments of inertia if computed by eq. 29 (expression of the moment of inertia for small oscillation angles) or by eq. 28 (expression of the moment of inertia for large oscillation angles) as function of motion amplitude. Colors refer to the contributions of each coefficient of eq. 28.

related to the nonlinear terms of the potential energy of the heave motion of the mass of the pendulum. When a small radius of gyration and a large ratio R/L are considered (Fig. 5b), the most influential terms are $P_1\left(\theta_0\right)$ and $P_2\left(\theta_0\right)$. These terms are related to the kinetic energy of the heave motion of the mass of the pendulum. In fact, for a large ration R/L the vertical velocity of the pendulum grows increasing the fraction of kinetic energy related to the motion of the mass. At the same time, if the radius of gyration is small, the kinetic energy related to the rotational motion of the pendulum is relatively small with respect to the kinetic energy related to its vertical motion. When these two conditions are present (Fig. 5b), the kinetic energy related to the vertical motion cannot be neglected, as usually done [14,18].

3.2 Virtual calibration

In this section a numerical calibration of the trifilar pendulum is performed in order to evaluate the capability of eq. 28 of actually measure the moment of inertia for large oscillations of the motion of the pendulum, i.e. the identifiability properties of the proposed model [21]. Also, the performances of the calibration model of eq. 28 are compared with the calibration formula proposed in [14,18] in which the term proportional to m is not considered.

For this analysis, the same multibody model described in Sect. 2.1 is used. For the virtual calibration, 10 bodies are considered, whose mass and inertia are reported in table 2. The first body represents the tare of the test rig and have null mass and inertia. Of the ten bodies of table 2, eight are used for the actual calibration of the test rig parameters (eq. 28). The other two bodies (bodies 5 and

Table 2: Mass and inertia of the bodies used for the calibration of the test rig.

Body number	Mass [kg]	Inertia [kg^2]	Radius of gyration [m]
1 (only tare)	0	0	-
2	1.615	0.0257	0.126
3	3.321	0.0423	0.113
4	3.321	0.0837	0.159
5	19.972	0.3321	0.129
6	19.972	0.2197	0.105
7	21.588	0.3487	0.127
8	21.588	0.2454	0.107
9	23.203	0.4158	0.134
10	23.203	0.3035	0.114

8) are used as verification, i.e. their inertia is computed by eq. 34 and compared to the nominal value to compute the error.

In Fig. 6 the results of the virtual calibration of the test rig based on eq 28 are reported for different values of the ratio R/L and of the radius of gyration ρ. The percentage error is computed with respect to the full scale of the test rig, considered equal to the maximum inertia considered in the calibration. The ratio R/L has been varied by keeping fixed L at its nominal value of table 1 and changing R accordingly. The radius of gyration has been varied by keeping the values of the masses of the calibration bodies at their nominal values of table 2 and multiplying by 9 their moments of inertia. The figure shows that the identifiability error due to the structure of the proposed model is low in all the considered conditions. In particular, the larger error, of the order of 0.1% of the full scale of the test rig, is found for a very high value of the ration R/L, a small radius of gyration ρ and large oscillation angles (Fig. 6b). This situation is the most demanding situation, in which a very high dependence of the oscillation period has to be expected from the oscillation angle as shown in Fig. 3. If the ration R/L is reduced or if the radius of gyration is increased, a large reduction of the error is shown (Fig. 6a, 6c and 6d).

In [18], a calibration procedure similar to the one proposed in Sect. 2 has been presented where the term function of m and the dependency on the amplitude have been neglected. Recently in [14], the same formula has been reproposed but showing that all the tests have to be performed with the same amplitude. The calibration formula, if m is neglected and for the same amplitude for all tests, reads [14]

$$J_1 = C_1 + C_2\left(\theta_0\right) T^2 + C_3\left(\theta_0\right) m_1 T^2 \tag{35}$$

where C_1, C_2 and C_3 can be determined with a procedure similar to the one of eq.s 30-eq 33. In Fig. 7 the results of the virtual calibration of the test rig based on eq 35 are reported for different values of the ratio R/L and of the radius of gyration ρ. The figure shows that this model gives the same results of the model of eq. 28 when the ration R/L is small (Fig. 7a and 7c). If this ratio grows, even for a relatively small value of R/L equal to 0.3, the model of eq. 35 shows decisively larger errors (Fig. 7b and 7d). These errors are mitigated as ρ grows (Fig. 7d.). This

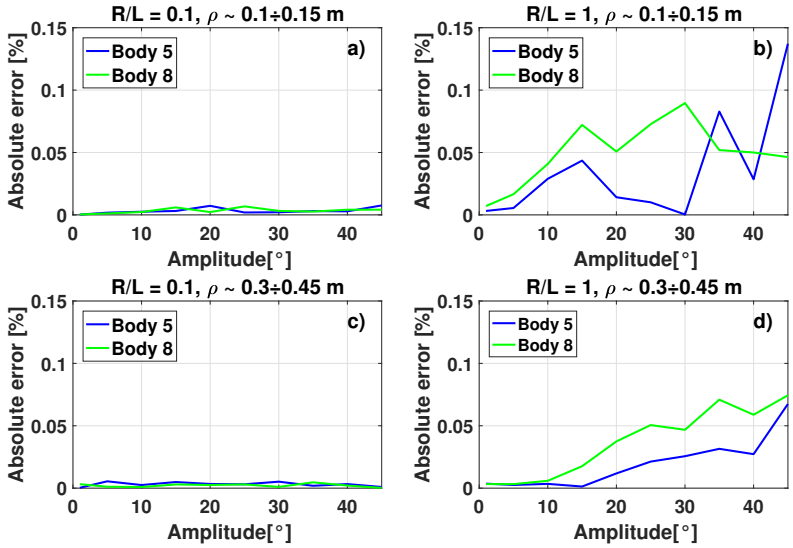

Fig. 6: Percentage errors in the virtual calibration of the test rig based on eq 28 for different values of the ratio R/L and of the radius of gyration ρ. Test rig data in table 1 and calibration masses data in table 2. The percentage error is computed with respect to the full scale of the test rig.

analysis shows that the term proportional to m has to be considered to correctly measure the moment of inertia for all the parameters combination, especially if R/L is large. It can be concluded that the model of eq. 28 is distinguishable from the model of eq. 35 [21].

4 Experimental calibration

The trifilar pendulum utilized for the experimental tests is shown in Fig. 8. The distance R is 0.162 m, the mass of the plate is 6.134 kg, its moment of inertia 0.086 kgm^2 and the radius of gyration 0.118 m. Three lengths of the cables have been considered: 0.976 m, 0.757 m and 0.446 m. The three corresponding ratios R/L are 0.166, 0.214 and 0.362. The cable lengths have been measured after the pendulum has been assembled. Such lengths result from the the assembling process, in which cable lengths have been adjusted to guarantee the horizontality of the plate.

The picture shows that the cables are clamped to the plate and to the support structure, so a structural torsional stiffness is present. The torsional stiffness of the cables has not been measured but has been roughly estimated around 0.05 Nm/rad for the unloaded pendulum. The precise knowledge of the value of the cable stiffness is not required, as it will be determined during the calibration procedure and included in the coefficient $P_1(\theta_0)$ of eq. 28. Also, as the cables are made by wire ropes, their torsional stiffness depends on the actual tension [23]. This dependence is mostly proportional to the load, i.e. for the trifilar pendulum to

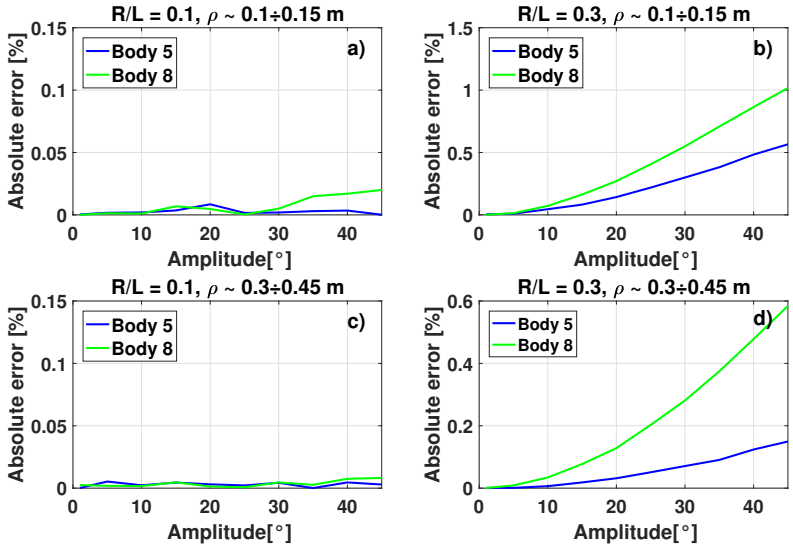

Fig. 7: Percentage errors in the virtual calibration of the test rig based on eq 35 for different values of the ratio R/L and of the radius of gyration ρ. Test rig data in table 1 and calibration masses data in table 2. The percentage error is computed with respect to the full scale of the test rig.

the mass of the pendulum. This dependence can be easily included in the coefficient $P_2(\theta_0)$ of eq. 28 and thus considered in the proposed calibration model.

The carrying plate has 8 calibrated holes disposed along a rectangle as shown in Fig. 8c. These holes are used to position calibrated masses (2 of about 10 kg and 4 of about 0.8 kg) at known locations in order to obtain the 10 bodies of table 2. The six masses used for the calibration have been manufactured in stainless steel with tight tolerances and accurately weighted and measured after manufacturing. The masses have a cylindrical shape and have a cylindrical centering surface with the diameter correspondent to the diameter of the positioning holes of the plate. The masses are used for the calibration of test rigs for the measurement of the inertia properties of rigid bodies [5], are part of a quality certification process according to the ISO 9001 standard [9] and approved by a third party certification agency. The calibrated masses employed for the calibration and configured to obtain the inertia properties of body 9 of Table 2 are shown in Fig. 8b.

The alignment of the centre of gravity of the bodies is guaranteed by the machined holes and verified by a balancing method [19,17,15]. The carrying plate is instrumented by a gyro (full scale 300 °/s) to measure the yaw oscillations and two monoaxial capacitive accelerometers (full scale 3 g) to check the lateral motion of the plate (Fig. 8a). The motion amplitude has been obtained by integrating the gyro signal. No centering device to avoid lateral displacements of the pendulum is present. The horizontality of the plate has been measured by a precision level and is within $\pm 0.1^o$ in all directions for all the considered cable lengths.

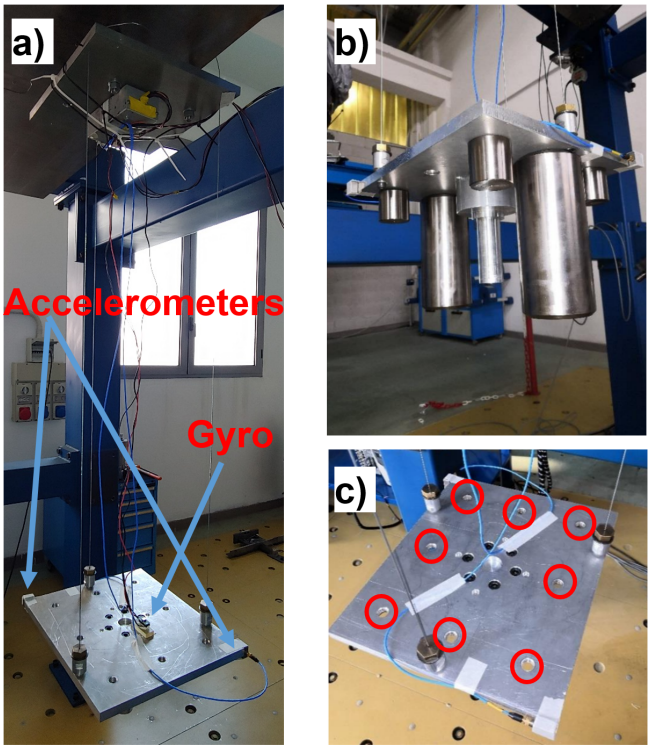

Fig. 8: Trifilar pendulum. a) Test rig view and instrumentation. b) Calibrated masses configured for body 9 of Table 2. c) Location of the calibrated holes on the plate (calibrated holes highlighted by red circles).

For each calibrated masses configuration of Table 2 and each cable length, from 5 to 10 tests have been performed. In each test, the pendulum has been displaced from rest of about 50^{o} and then released. The motion has been acquired at 2000 Hz. Each test has been acquired until the motion amplitude has reduced below 5^{o}. In this way, from the acquired data, different motion amplitudes can be considered for the calibration of the test rig. The damping has been computed for all tests by a logarithmic decay approach and, depending on the actual calibrated mass and cable length, values between 0.02% and 0.17% of the critical damping have been found. These values are quite small and do not have any effect on the period of the pendulum. The accelerometer signals have been examined to check if evident lateral motions were present. In none of the tests significant lateral motions have been found, meaning than lateral motions are not relevant when large oscillation amplitudes are considered. A reasonable attention of the operator is sufficient to keep such motions small, and negligible, with respect to the large oscillations considered.

In Fig. 9 the measured periods for ten tests of body 1 and ratio R/L equal to 0.214 are shown for three different motion amplitudes. The figure shows the very good repeatability of the measurements. The measured periods fit very well a normal distribution and the standard deviation is of the order of milliseconds.

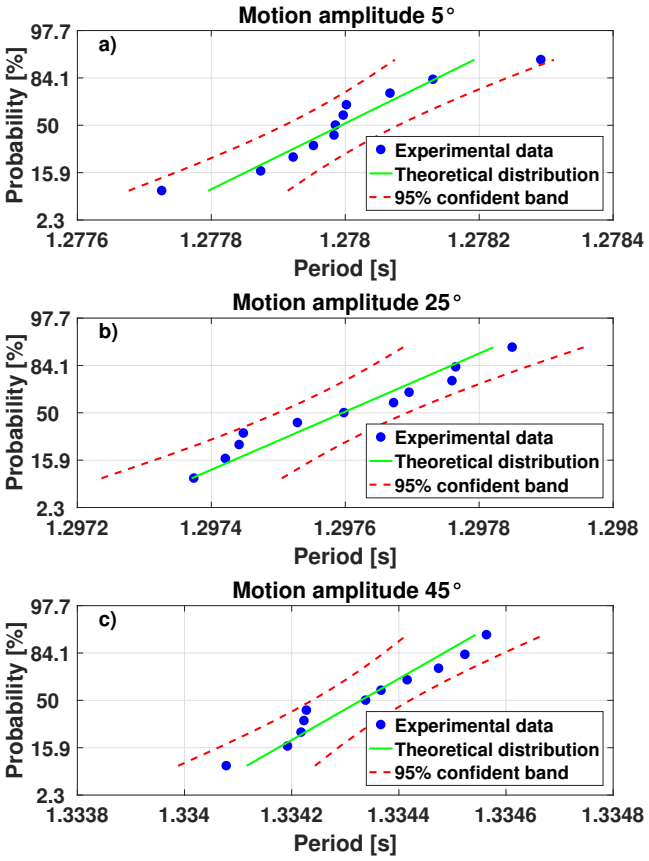

Fig. 9: Normal probability plot of the measured period values, body 1, $R/L = 0.214$. a) Motion amplitude 5^o. b) Motion amplitude 25^o. c) Motion amplitude 45^o.

Fig. 10 shows the measured moments of inertia with respect to their reference value. The figure has been reported for the most nonlinear condition of the tests, represented by the higher value of the R/L ratio at the maximum considered angle. Similar pictures can be derived for all the other tested conditions. The moments of inertia of the eight calibration bodies and the two verification bodies all lay on the straight line at 45^o. The coefficients of the interpolating line have been computed by considering only the eight calibration bodies and the figure shows that the two verification bodies lay very well on the same line.

The absolute percentage error between the measured and reference values of the moments of inertia of the verification bodies normalized with respect to the full scale of the test rig is reported in Fig. 11. The percentage error is not function of the oscillation angle considered and it is actually constant with the oscillation angle. The percentage error is of the order of 0.1%, in most cases well below this value. When the shortest cables are used, due to the clamping constraints, a s-shape deformation of the cables was present and, especially for higher values of

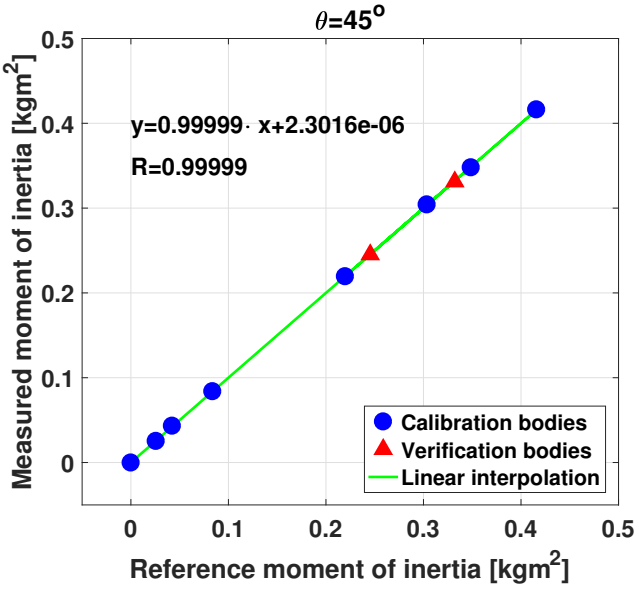

Fig. 10: Test rig linearity, $R/L = 0.362$, oscillation amplitude of 45°.

inertia, a slightly increase in the errors on the measurements has been found. In all the considered cases, no dependence of the error on the amplitude can be seen.

Finally, in Fig. 12 the absolute percentage error in the calibration of the test rig based on eq 35 and $R/L = 0.362$ is depicted. If a calibration formula neglecting the term proportional to m is employed, although a relatively small error is still obtained, a clear dependency of the calibration error on the motion amplitude is observed. This non linear effect is more evident in the results for body 8 and could be due to a smaller radius of gyration of this body. For highly nonlinear motions, the three parameters calibration of eq. 35 is not able to correctly model the system.

Conclusion

In this paper the large oscillations of the trifilar pendulum have been investigated with the aim to derive a calibration procedure for the measurement of the moment of inertia exploiting this kind of motion. An analytical formula relating the oscillation period to the motion amplitude has been derived. This analytical model has shown that the period of oscillation is more affected by the motion amplitude when the radius of gyration of the pendulum is small or when the cables are relatively short with respect to their distance.

The derived analytical formula has been employed for the definition of a calibration procedure able to measure the moment of inertia when the motion is large and the period is strongly dependent on the motion amplitude. It has been shown that four calibration constants have to be identified for the correct calibration of the test rig. With respect to well established calibration procedures considering

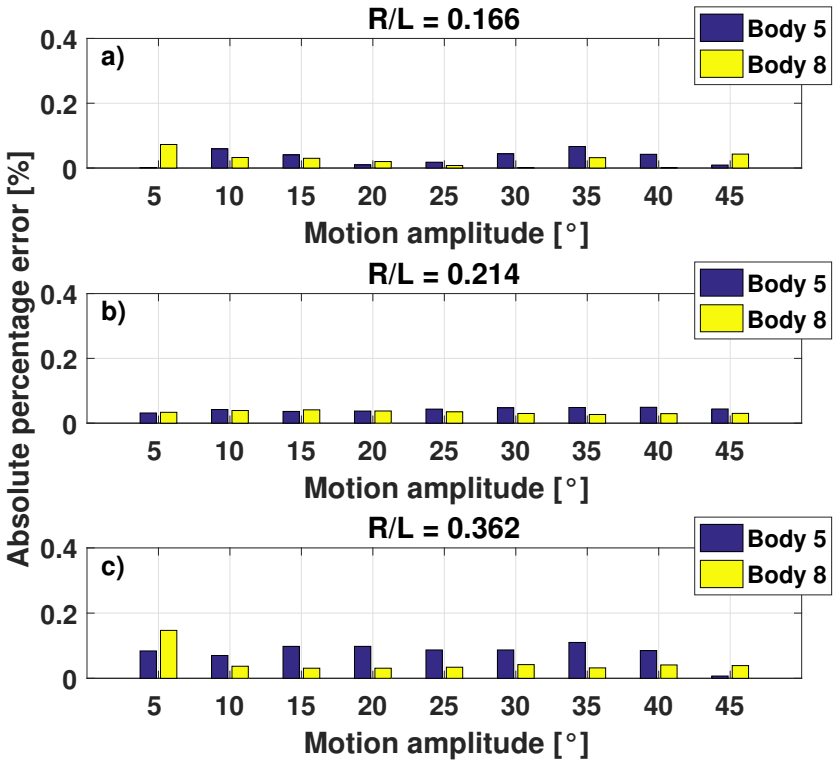

Fig. 11: Percentage errors in the calibration of the test rig based on eq 28 for 3 different values of the ratio R/L. Test rig data in table 1 and calibration masses data in table 2. The percentage error is computed with respect to the full scale of the test rig. a) $R/L = 0.166$. b) $R/L = 0.214$. $R/L = 0.362$.

only three parameters, an additional parameter function of the mass of the body under investigation has been found.

An experimental campaign with a trifilar pendulum with three different cables lengths has shown that the proposed procedure is able to compensate the effects of the large oscillation nonlinearities for angles up to 45°. For the tests, ten compact bodies with small radii of gyration have been considered. A very good accuracy of the order of 0.1% of the full scale of the test rig has been obtained with a very simple hardware. In fact, in the analytical model also the contribution of the torsional structural stiffness of the system has been included, allowing the realization of the pendulum with clamped wires without complex spherical joints. A very simple instrumentation composed by only one gyro is necessary for the measurement.

Finally, it has been shown that for the shortest cable length, the nonlinear effects of the amplitude are relevant and if a standard three parameters calibration

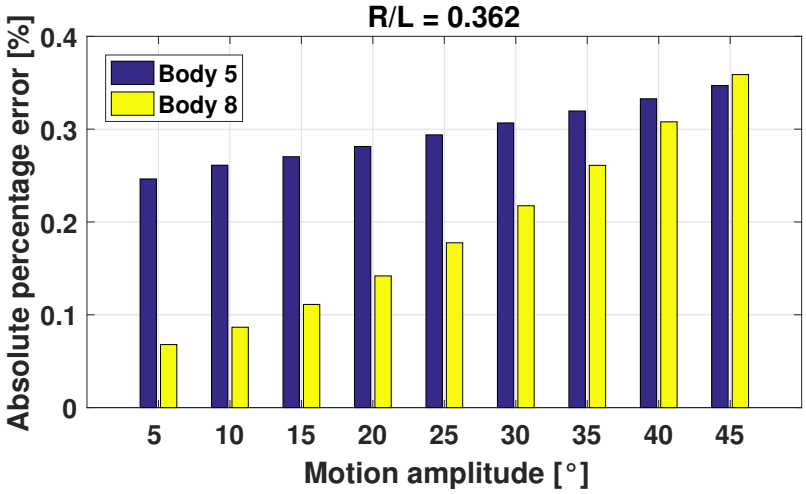

Fig. 12: Percentage errors in the calibration of the test rig based on eq 35 for $R/L = 0.362$. Test rig data in table 1 and calibration masses data in table 2. The percentage error is computed with respect to the full scale of the test rig.

model is employed, a clear dependency of the accuracy with amplitude has been found.

References

1. Acton, J.R.: Solving Equations with Physical Understanding. Taylor & Francis, London (1985)
2. Björck, Å.: Numerical methods for least squares problems. Society for Industrial and Applied Mathematics, Philadelphia U.S.A. (1996)
3. du Bois, J.L., Lieven, N.A.J., Adhikari, S.: Error analysis in trifilar inertia measurements. Experimental Mechanics **49**(4), 533–540 (2009). DOI 10.1007/s11340-008-9142-4
4. Genta, G., Delprete, C.: Some considerations on the experimental determination of moments of inertia. Meccanica **29**(2), 125–141 (1994). DOI 10.1007/BF01007497
5. Gobbi, M., Mastinu, G., Previati, G.: A method for measuring the inertia properties of rigid bodies. Mechanical Systems and Signal Processing **25**(1), 305–318 (2011). DOI 10.1016/j.ymssp.2010.09.004
6. Hinrichsen, P.F.: Analysis of Bi and Trifilar Suspension Oscillations (2015). DOI 10.13140/RG.2.1.3566.3527
7. Hinrichsen, P.F.: Bi and trifilar suspension centering correction. Meccanica **53**(1-2), 21–32 (2018). DOI 10.1007/s11012-017-0700-7
8. Hou, Z.C., ning Lu, Y., xin Lao, Y., Liu, D.: A new trifilar pendulum approach to identify all inertia parameters of a rigid body or assembly. Mechanism and Machine Theory **44**(6), 1270–1280 (2009). DOI 10.1016/j.mechmachtheory.2008.07.004
9. ISO-9001:2015: Quality management systems—requirements (2015)
10. Jardin, B.M.: Improving Mass Moment of Inertia Measurements. Mathworks Technical Articles and Newsletters pp. 1–8 (2018)
11. Jardin, M.R., Mueller, E.R.: Optimized Measurements of Unmanned-Air-Vehicle Mass Moment of Inertia with a Bifilar Pendulum. Journal of Aircraft **46**(3), 763–775 (2009). DOI 10.2514/1.34015
12. Korr, A., Hyer, P.: A trifilar pendulum for determination of moments of inertia. Tech. rep., Armed Services Technical Information Agency, Arlington, Virginia (1962)

13. Lyons, D.P.: Obtaining Optimal Results with Filar Pendulums for Moment of Inertia Measurements. In: 61st SAWE Annual Conference, Virginia Beach, Virginia, May 18-22, 3237, p. 29 (2002)
14. Previati, G., Ballo, F.: Trifilar pendulum: non-small oscillations and calibration. In: 78th SAWE International Conference on Mass Properties Engineering, pp. 1–16. Norfolk, Virginia (2019)
15. Previati, G., Ballo, F.M., Gobbi, M.: A Portable Device for Measuring the Cog: Design, Error Analysis and Calibration. In: SAWE technical paper n.3752 (2020)
16. Previati, G., Gobbi, M., Mastinu, G.: Measurement of the inertia tensor - A review. In: 73rd Annual Conference of the Society of Allied Weight Engineers, Inc., SAWE 2014, pp. 1–23. Society of Allied Weight Engineers (2014)
17. Previati, G., Gobbi, M., Mastinu, G.: Moments of inertia and products of inertia of a rigid body - Design principles of measurement systems. Society of Allied Weight Engineers, Los Angeles, CA, USA (2018)
18. Ringegni, P.L., Actis, M.D., Patanella, A.J.: An experimental technique for determining mass inertial properties of irregular shape bodies and mechanical assemblies. Measurement: Journal of the International Measurement Confederation **29**(1), 63–75 (2001). DOI 10.1016/S0263-2241(00)00028-2
19. Schedlinski, C., Link, M.: A survey of current inertia parameter identification methods. Mechanical Systems and Signal Processing **15**(1), 189–211 (2001). DOI 10.1006/mssp.2000.1345
20. Tang, L., Shangguan, W.B.: An improved pendulum method for the determination of the center of gravity and inertia tensor for irregular-shaped bodies. Measurement: Journal of the International Measurement Confederation **44**(10), 1849–1859 (2011). DOI 10.1016/j.measurement.2011.09.004
21. Walter, E., Pronzato, L.: Identification of parametric models from experimental data. Springer, London (1997)
22. Williams, H.: Measuring the Inertia Tensor. In: IMA MAthematics 2007 Conference. London (2007)
23. Xiang, L., Wang, H.Y., Chen, Y., Guan, Y.J., Wang, Y.L., Dai, L.H.: Modeling of multi-strand wire ropes subjected to axial tension and torsion loads. International Journal of Solids and Structures **58**, 233–246 (2015). DOI 10.1016/j.ijsolstr.2015.01.007